This is a repository copy of *Vitrification of an intermediate level Magnox sludge waste*.

Article:

Vitrification of an intermediate level Magnox sludge waste

Shengheng Tan[1,*], Nick Kirk[2], Martyn Marshall[2], Owen McGann[2] and Russell J Hand[1,†]

[1]ISL, University of Sheffield, Department of Materials Science & Engineering, Sir Robert Hadfield Building, Mappin Street, Sheffield, S1 3JD, UK

[2]Glass Technology Services, 9 Churchill Way, Chapeltown, Sheffield, S35 2PY, UK

Abstract

A novel iron containing alkali alkaline earth borosilicate glass has been developed that can vitrify up to 30 wt% (dry weight) of a Magnox sludge waste in a homogeneous wasteform at a melting temperature of 1200°C. Ce was used as a simulant of the actinide content in the waste. The waste was spiked with 0.5wt% of Cs_2O of which 90% was retained in the glass. 60% of the Cl was also retained. Mg content limited the waste loading as loadings in excess of 30wt% led to the formation of forsterite and in some cases CeO_2 and $MgFe_2O_4$ based spinels. PCT leach testing of the glasses for periods up to 180 days indicated the formation of an amorphous magnesium (alumino-)silicate hydrated layer on the glass surface together with barium rich crystalline precipitates. No Ce was detected in the leachate.

1. Introduction

In the UK intermediate level radioactive waste (ILW) is categorised as a waste which has an activity that exceeds 4×10^9 Bq t^{-1} (α) and/or 12×10^9 Bq t^{-1} (β and γ) but

* Now at China Institute of Atomic Energy; P.O. Box 275 - 93, China Institute of Atomic Energy, Beijing, 102413, China
† E-mail: r.hand@sheffield.ac.uk

does not generate a level of heat (<2 kW m^{-3}) that has to be taken into consideration [1]. In the UK, the estimated total volume of ILW is 290,000 m^3 (99,000 m^3 produced by 2016 and 191,000 m^3 to be produced in the future) [2], accounting for 6.4% of the total nuclear waste volume. ILW consists of a wide range of wastes including contaminated steels, graphite, concrete and sand, sludges, ion exchange resins, flocs and Pu-contaminated materials [1-3]. Historically in the UK ILW has been immobilised by encapsulation into cementitious materials [4-6]; however this route is not suitable for all UK ILW. In addition cementation results in a largely increased waste volume [7], which results in higher long-term storage and disposal costs. In comparison, vitrification, which is currently used in the UK to immobilise high level waste (HLW) [8-12], provides notable waste volume reduction and more durable end products than cementation. If applied to ILW these significant advantages can override the higher operational costs associated with a thermal treatment process.

One of the more challenging ILWs for vitrification is the Magnox sludge waste from the fuel storage ponds at Sellafield. Heath *et al.* [13] have recently reported successful immobilisation of a Magnox sludge simulant into a glass-ceramic wasteform using hot isostatic pressing (HIP); however in that study a rather simple simulant (a pure Mg(OH)$_2$ slurry) was used. This paper describes the development of novel glasses for the vitrification of a more complex Magnox sludge simulant (containing minor components and metals), which is compositionally a better analogue to the actual waste stream. The development work was carried out as part of the Innovate UK funded Hazmelt project, in which a novel furnace technology for the vitrification of nuclear wastes was developed.

2. *Experimental*

2.1. Waste simulant

The target Magnox sludge waste stream contains a significant amount of Mg (as metal and as hydroxide) and U, with an additional challenge arising from a notable Cl content (~4 mol%). For the inactive development work a waste simulant was prepared (see Table 1). Ce was used as a surrogate for both U and Pu and stable isotopes of Cs and Sr were used instead of the radioactive isotopes present in the actual sludge waste. To enable detection the Cs and Sr loadings (as Cs_2O and SrO) in the simulant were deliberately elevated to 0.5 wt% compared to <0.001 wt% in the actual Magnox sludge. Apart from Mg and $Mg(OH)_2$, which are both present in the waste, other components have been added in chemically convenient forms intended to ensure that the chemical composition of the waste is correctly simulated after melting. No attempt was made to simulate the water content of the waste.

Table 1 Composition of the Magnox sludge simulant

Component	wt%	mol%	Component	wt%	mol%	Component	wt%	mol%
$Mg(OH)_2$	58.91	70.39	KCl	1.65	1.54	$BaCO_3$	0.13	0.05
Mg (metal)	2.73	7.83	NaCl	2.51	2.99	TiO_2	0.09	0.08
CeO_2[†]	20.39	8.25	Na_2SO_4	1.17	0.57	ZnO	0.18	0.15
$Al(OH)_3$	2.37	2.12	Na_3PO_4	0.32	0.14	Cs_2O[‡]	0.5	0.12
$CaCO_3$	5.61	3.91	NiO	0.05	0.05	SrO[‡]	0.5	0.34
Fe_2O_3	1.25	0.55	Cr_2O_3	0.1	0.05	PbO[*]	-	-
K_2CO_3	1.45	0.73	CuO	0.12	0.16			

[†] Substituted on a molar basis for actinides (primarily U) present in the actual sludge waste.

[‡] 0.5 wt% each of Cs_2O and SrO were added as spikes in the simulant. In the real waste their concentrations are < 0.001 wt%

[*] 0.19 wt% PbO present in the actual sludge waste was omitted from the simulant.

2.2.Sample preparation

A preliminary study was conducted on a range of borosilicate glasses (see Table 2) using a simplified 9:1 molar $Mg(OH)_2$/Mg simulant. This indicated that of the glasses

tested the $5Li_2O$-$5Na_2O$-$5CaO$-$15BaO$-$7.5Fe_2O_3$-$12.5B_2O_3$-$50SiO_2$ (mol%) glass, labelled HM09, had the highest capacity for waste loading. Thus this glass was selected for the fuller investigation detailed in this paper.

Table 2: Glasses considered in the preliminary study (compositions in mol%). All compositions melted at 1200°C unless otherwise stated

	Li_2O	Na_2O	CaO	BaO	Fe_2O_3	Al_2O_3	B_2O_3	SiO_2	Outcome
HM01	7.80	5.64	11.08	18.24	2.92	0.38	2.23	51.71	Inhomogeneous melt at 20 wt% loading
HM02	9.16	5.68		16.33	4.90	0.38	5.62	57.93	As above
HM03	17.90	8.63		8.72	3.35		5.76	55.64	Separated layer on the melt surface
HM04	0.91	2.75	2.38	9.04	24.24		5.94	57.42	Did not melt until 1300 °C at 26.7 wt% loading
HM05		3.36		22.36	8.63		8.10	57.55	Could not be poured at 25 wt% loading
HM06	13.45	3.72	7.76	5.60	8.70		9.66	51.11	Inhomogeneous at 25 wt% loading
HM07	5.00	5.00		20.00	7.50		12.50	50.00	Inhomogeneous at 30 wt% loading
HM08	14.09	3.40	7.51	5.49	8.57		9.57	51.38	Failed at both 20 and 25 wt% loading
HM09	5.00	5.00	5.00	15.00	7.50		12.50	50.00	Maximal 35 wt% loading; phase separated at 40 wt%
HM10		18.75			6.25		12.50	62.50	Maximal 27 wt% loading
HM11		18.75			12.50		6.25	62.50	Maximal 25 wt% loading
HM12	5.00	15.00	7.50	7.50	7.50		7.50	50.00	Maximal 30 wt% loading

Glass raw materials to produce 100 g glass were mixed with waste simulant and thoroughly homogenised; the glass raw materials were high purity glass making sand

(SiO_2, Loch Aline sand, Tilcon, UK) and laboratory grade H_3BO_3, Fe_2O_3, Li_2CO_3, Na_2CO_3, $CaCO_3$ and $BaCO_3$ (all from Fisher Scientific UK). Sample naming takes the form HM09-xMS where x indicates the waste loading in wt%. The mixture was placed in a mullite crucible and heated in an electric furnace to 1200 °C and held at that temperature for 2 h, prior to being poured into a pre-heated steel mould and transferred to an annealing furnace. The cast glass blocks were annealed at 550 °C for 1 h and cooled to room temperature at 1 °C min^{-1}.

2.3. Characterisation

X-ray diffraction (XRD) and differential thermal analysis (DTA) measurements were performed on crushed glass powders passing a 75 µm sieve, using a Bruker D2 Phaser X-ray Diffractometer (CuKα at 30 kV and 10mA, $2\theta = 10\text{-}70°$, step size 0.05°) and a Perkin Elmer STA8000 machine (room temperature to 1000 °C at 10 °C min^{-1}, Pt crucible, static air flow), respectively. Glass powders were also used for compositional analysis by inductively coupled plasma mass spectroscopy (ICP-MS).

The as-prepared glasses were sectioned to produce slices ~5 mm thick. One surface of the slices was successively ground and polished using 400 to 1200 SiC grit papers, and 6 to 1 µm diamond suspensions. After thorough rinsing with isopropanol Raman spectroscopy and scanning electron microscopy (SEM) was conducted on the polished slices. Raman spectroscopy was carried out with a Renishaw Invia Raman spectrometer equipped with a CCD detector (514.5 nm green line laser at 20 mW, ×50 objective, 0-2000 cm^{-1} scanning range, 10s exposure time and 10 accumulations). Calibration with silicon was undertaken each time the spectrometer was used. Scanning electron microscopy (SEM) was carried out on carbon coated samples, using either HITACHI TM3010 SEM equipped with an energy dispersive X-ray spectrometer (EDS) for compositional analysis and elemental mapping or an FEI

Inspect F/F50 SEM machine for images at higher magnifications and EDS line scans. The latter machine was operated at 15 kV with a spot size of 3.0. Glass chemical durability was investigated using the Product Consistency Test B (PCT-B) following the procedures described in ASTM C1285-02 (2008). The prepared glass powders were sieved to be between 75 and 150 μm, rinsed with deionised water and isopropanol alternatively for 10 times and dried the powders at 95 ℃ for 48 hours. Fines removal was achieved by immersing the beaker containing glass powders and isopropanol into an ultrasonic bath 3 times for 1 min. Testing was carried out in PFA TFE-fluorocarbon vessels at a SA/V ratio of 1200 m^{-1} and lasted for up to 180 days.

3. Results

3.1. Loading capacity and glass composition

HM09 glass with up to 30 wt% waste loading remained homogeneous. Higher waste loadings resulted in phase separation within glass; this was a slightly lower limit for homogeneity than was seen with the simplified simulant in the preliminary study. At 35 and 40 wt% loadings (HM09-35MS and HM09-40MS) only small amounts of separated phases were observed while at 45 wt% loading (HM09-45MS) there was a significant amount of phase separated material throughout the glass matrix. The maximal amount of the simulant waste that can be loaded to HM09 glass while not causing visible phase separation was therefore determined to be 30 wt%.

Table 3 Analysed HM09 glass compositions*

Component (mol%)	HM09-						
	Nominal (0MS)	0MS	10MS	20MS	30MS	40MS	45MS
SiO_2	50.00	46.11	43.19	43.01	40.58	38.61	
B_2O_3	12.50	11.88	10.88	9.35	8.60	8.30	
Fe_2O_3	7.50	7.89	7.13	5.97	5.37	5.28	
Al_2O_3		5.39	1.17	0.98	0.87	1.02	
Li_2O	5.00	4.23	3.80	3.31	3.04	2.97	
Na_2O	5.00	4.25	3.89	3.54	3.58	3.39	

K$_2$O		0.27	0.27	0.32	0.31	0.39	
MgO		0.16	9.60	14.98	19.48	22.15	
CaO	5.00	5.45	5.56	5.22	5.19	5.35	
SrO		0.06	0.14	0.17	0.17	0.16	
BaO	15.00	14.15	13.04	11.10	9.95	9.94	
CeO$_2$		<0.01	0.80	1.16	1.40	1.68	
SO$_3$		<0.01	0.12	0.11	0.13	0.14	
Cl		0.02	0.29	0.62	1.22	0.43	
Cs$_2$O		<0.01	0.01	0.03	0.04	0.05	
Others**		0.12	0.11	0.13	0.07	0.14	
Total	100.0	100.0	100.0	100.0	100.0	100.0	
Density (g/cc)		3.278	3.319	3.309	3.291	3.305	3.309
T$_g$ ($\pm5°C$)		514	527	541	545	554	556
T$_L$ ($\pm5°C$)		980			1082		

*All elements except Cl were analysed by ICP-MS; Cl content was obtained from EDS.
**Others may include ZnO, CuO, TiO$_2$, MnO, NiO, Cr$_2$O$_3$ and P$_2$O$_5$.

Glass compositions measured by ICP-MS (Cl content by EDS) are presented in Table 3. Given the presence of several anion species in the waste it is not possible to provide fully meaningful target oxide composition for the waste loaded glasses hence only the target composition of the base glass is given. It was concluded that mullite crucible had suffered severe attack from the base glass (HM09-0MS) during melting given the high Al$_2$O$_3$ content in the base glass (5.39 mol%); however the attack was notably suppressed with the addition of waste.

The retention rate of Cs and Cl in the glasses produced is plotted in Fig. 1. The glass shows a constant Cs retention rate of 90% at all waste loadings, regardless of whether the glass remained homogeneous. On the other hand, the Cl content in glass exhibits a roughly constant retention rate of approximately 60% up to the 30 wt% waste loading level; however this was followed by a significant decrease to a 22% retention rate at 40 wt% waste loading, where the glass is heterogeneous.
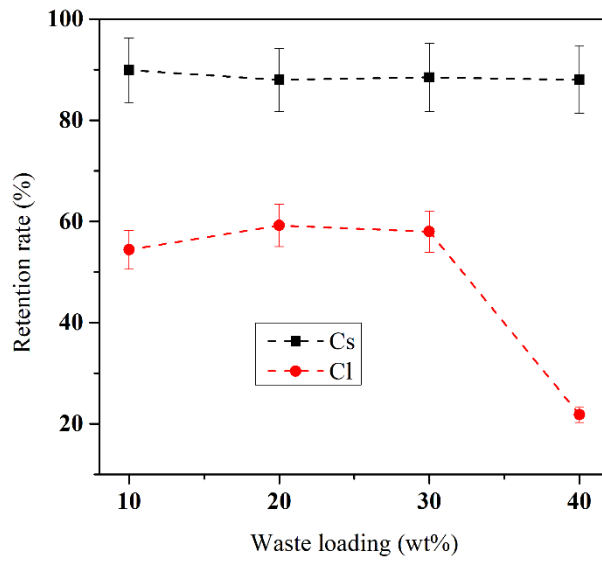
Fig. 1 Cs and Cl retention rates in waste loaded HM09 glass
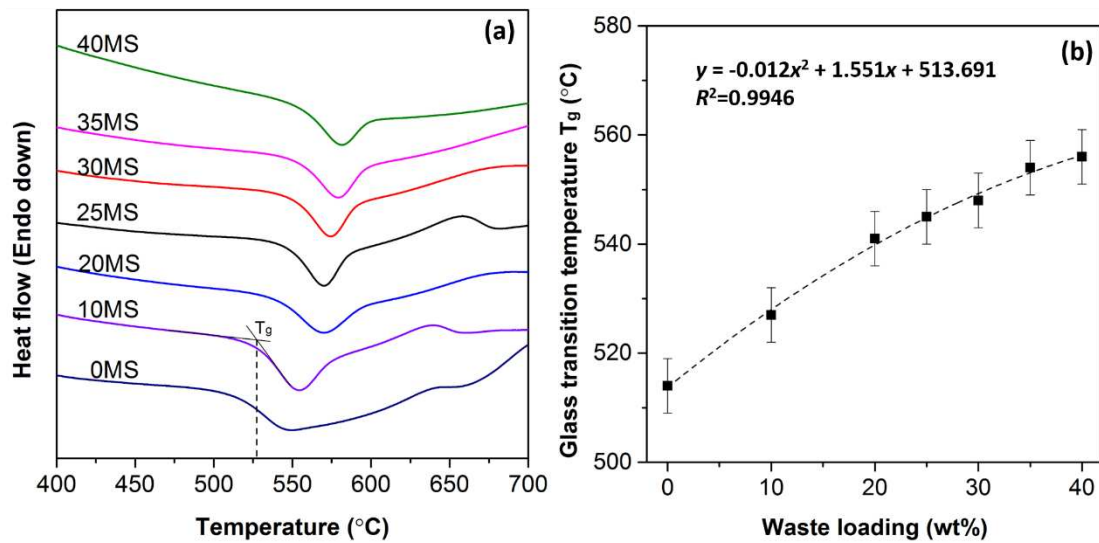
3.2. Thermal properties and crystallisation

Fig. 2 (*a*) DTA curves of HM09 glass with up to 40 wt% waste loading and (*b*) T_g

versus waste loading; the data is well fitted with a quadratic regression line

Fig. 2*a* shows the DTA curves of prepared glasses. The glass transition temperature

(T_g, estimated from the extrapolated onset of the first endothermic peak in the curves)

clearly increases with waste loading from 514 °C for the base glass to 556 °C for

HM09-40MS glass; and the data show a steady increase with increasing waste loading

in glass (Fig. 2*b*, best fitted with a quadratic regression line). Meanwhile, a small exothermic peak that is attributable to crystallisation is observed at ~650 ℃ for glasses with up to 30 wt% waste loading; at 35 and 40% wt% loadings this peak does not appear, presumably reflecting the fact that crystallisation has already occurred.
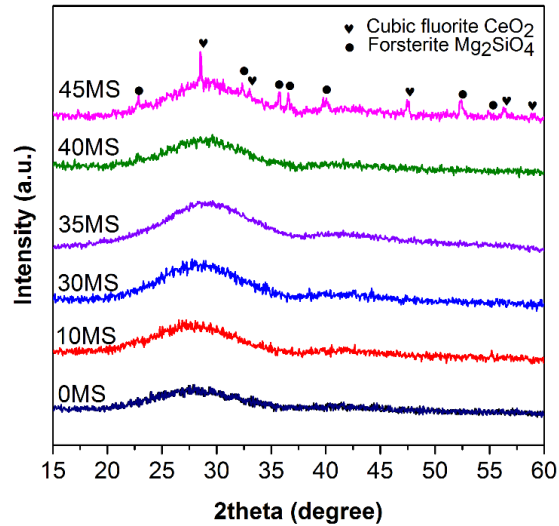

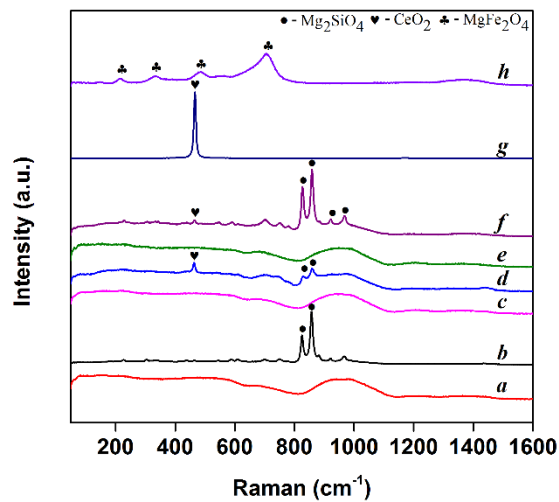Fig. 3 XRD patterns of HM09 glass with up to 45 wt% waste loading.

Fig. 4 Raman spectra of (*a*) HM09-35MS glassy region (*b*) HM09-35MS crystallised region (*c*) HM09-40MS glassy region (*d*) HM09-40MS crystallised region (*e*) HM09-45MS glassy region and (*f-h*) HM09-45MS crystallised regions.

As shown in Fig. 3, amorphous XRD patterns have been obtained for samples with up to 40 wt% waste loading while a number of crystalline peaks were recorded for HM09-45MS glass. These peaks are attributable to Mg_2SiO_4 (forsterite, PDF4#00-004-0768, at $2\theta = 22.8°$, $32.4°$, $35.7°$, $36.6°$, $40.0°$, $52.4°$ and $54.9°$) and CeO_2 (cubic cerium oxide PDF4#00-004-0593, at $2\theta = 28.5°$, $32.9°$, $47.5°$, $56.4°$ and $58.9°$), respectively. The absence of crystalline peaks in XRD patterns of phase separated HM09-35MS and 40MS glasses is likely because the amount of separated phases in them is low enough to be below the limits of detection by XRD. However, Raman spectra of the phase separated regions of these glasses do indicate the presence of crystals. The homogeneous glass and the glassy parts of the phase separated samples have Raman spectra like that shown in Fig. 4a, where the prominent broad band at 850-1150 cm^{-1} is assigned to Si-O asymmetric stretching vibrations and the minor band at 650-800 cm^{-1} is likely due to vibrations of four-coordinated boron or symmetric stretching vibrations of Si-O [14-16]. As shown in Fig. 4b, the separated phase in HM09-35MS glass is identified to be forsterite, based on the intense peaks at 825, 858 and 967 cm^{-1} which are assigned to different υ_3 modes of SiO_4^{2-} tetrahedra in Mg_2SiO_4 crystals [17, 18]. In HM09-40MS glass (Fig. 4d), an additional peak at 466 cm^{-1} is observed, which can be assigned to cubic CeO_2 crystals [19, 20]. In addition, one Raman spectrum taken from HM09-45MS glass (Fig. 4h) contains peaks at 215, 330, 484 and 706 cm^{-1} which are characteristic of $MgFe_2O_4$ spinel [21, 22], suggesting that $MgFe_2O_4$ spinels are also formed in certain crystallised regions of HM09-45MS glass.
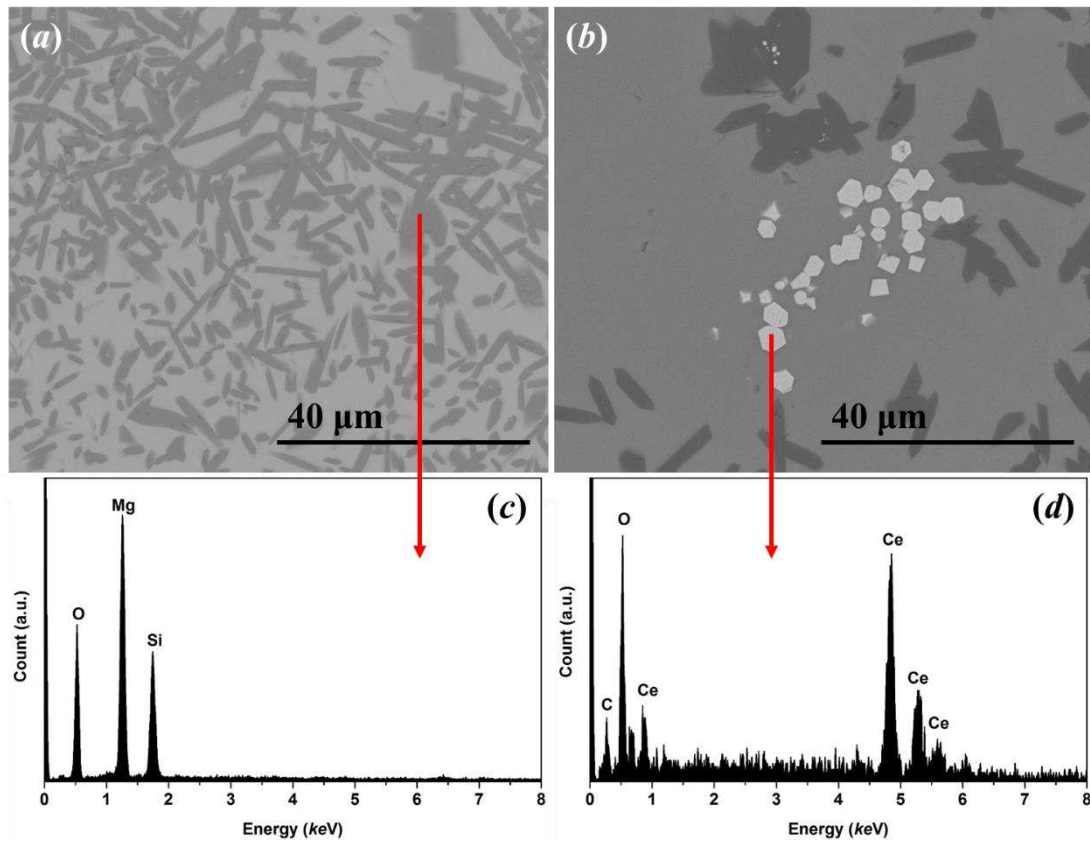
3.3. Microstructural investigations

Figure 5 (*a*) and (*b*): SEM images of separated phases in HM09-35MS and -40MS glass, respectively; (*c*) and (*d*): EDS spectra of corresponding phases.

The phase separation in HM09-35MS to HM09-45MS samples was investigated by SEM/EDS. As indicated in Figs. 5*a* and *c*, the separated phases in HM09-35MS are essentially plate-like and are composed of Mg, and Si, with a normalised formula of $Mg_{1.94}Si_{1.03}O_4$ (determined from EDS) which is approximate to Mg_2SiO_4, supporting the Raman results. As for the HM09-40MS sample, BSE imaging (Fig. 5*b*) demonstrates the presence of some bright facetted crystals in addition to Mg_2SiO_4 in the crystallised regions. These bright crystals are ~5 µm in size and based on EDS are CeO_2 (Fig. 5*d*) again supporting the Raman results (Fig. 4*e*). The heavily phase separated HM09-45MS sample contains a greater number of Mg_2SiO_4 and CeO_2 crystals than the HM09-35MS and HM09-40MS samples (Figs. 6a and b). In addition

grey tabular particles can be seen (Fig. 6*c)*, composed of Mg, Fe and O and with a formula of $Mg_{0.72}Fe_{2.18}O_4$ (likely to be the Mg ferrite spinel seen in Fig. 4*h*) near some Mg_2SiO_4 plates and a number of small particles (Fig. 6*d*) composed of Mg, Fe, Si and O, and thought likely to be olivine $(Mg,Fe)_2SiO_4$, although more evidence is required to be definitive about this, which are embedded in the Mg_2SiO_4 plates.
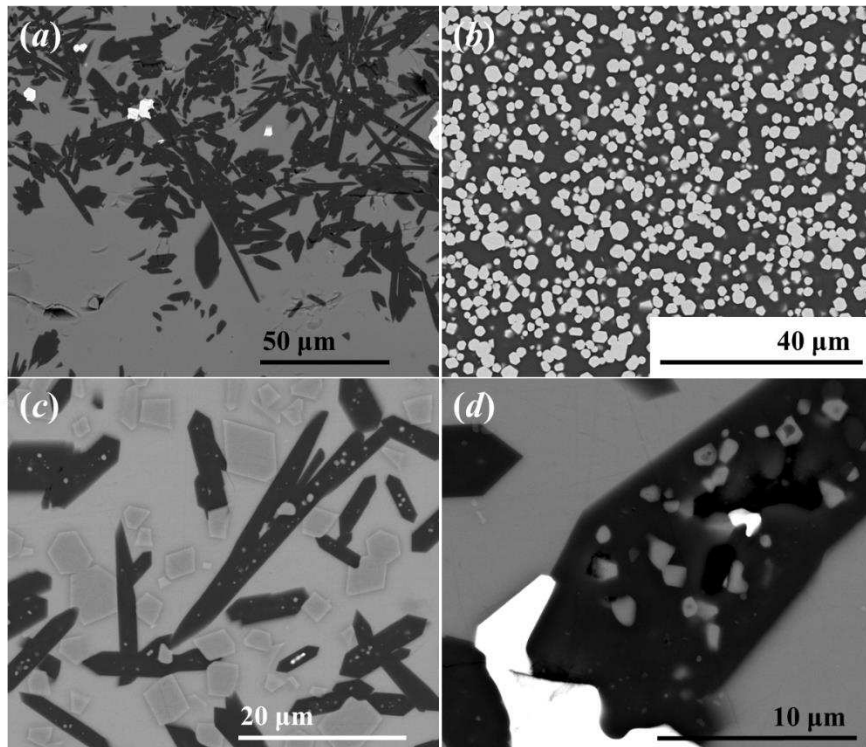

Figure 6 SEM images of separated phases in HM09-45MS sample.

Small amounts of Mg-rich particles have been found in crystallised regions in HM09-40MS and HM09-45MS (Fig. 7 shows an example in HM09-40MS). According to the elemental mapping, these small and round particles (<20 µm) only contain Mg and O, and many of them are in contact with a phase that is enriched in Fe, Mg and O, enclosed by the previously identified Mg_2SiO_4 plates. These Mg-rich particles are believed to be residual Mg granules (oxygen is likely introduced during sample preparation for SEM, confirmed by EDS analysis of the original Mg granules prepared using the same protocol).
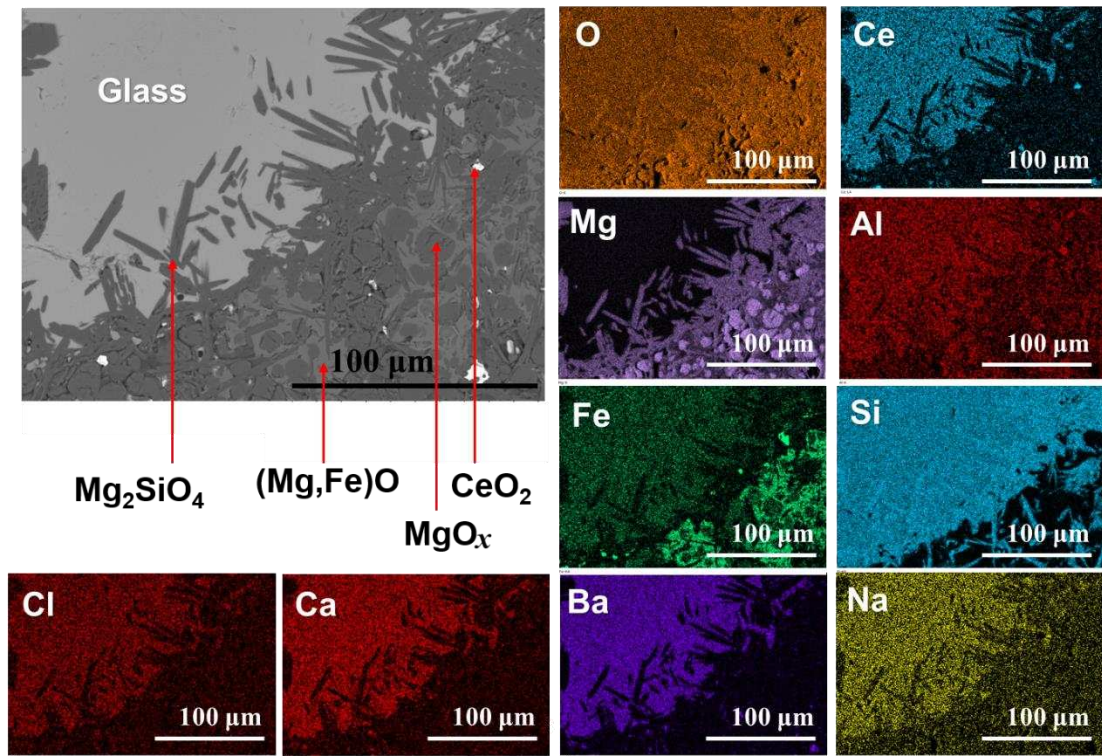
Fig. 7 EDS mapping of a crystallised region in HM09-40MS containing undissolved

Mg granules.

3.4. Durability testing (PCT-B)
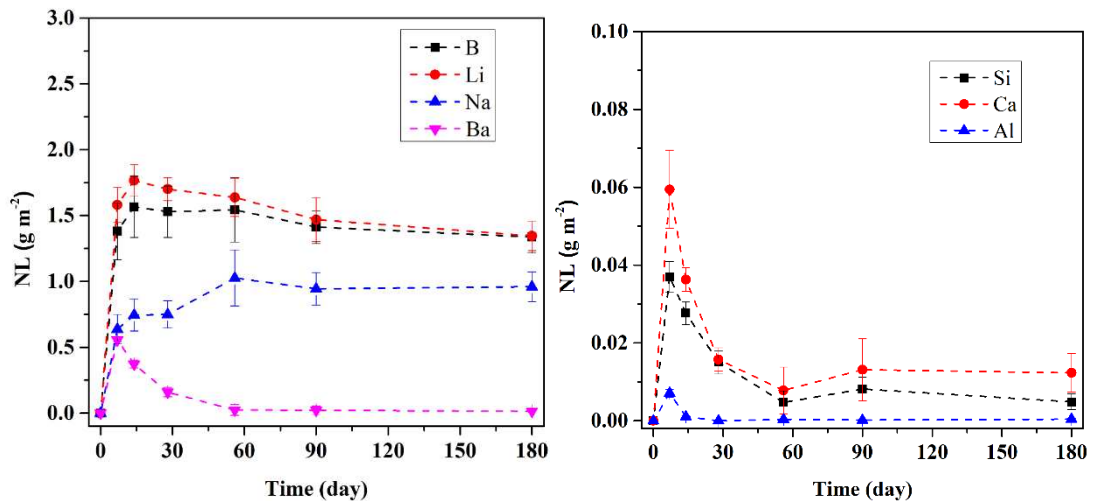
3.4.1. Leaching

Fig. 8 Normalised mass losses of (*a*) B, Li, Na and Ba and (*b*) Si, Ca and Al from

HM09-30MS during the PCT-B test.

The normalised mass losses of each element (NL_i) in HM09-30MS glass during the PCT-B test are plotted in Fig. 8a and b. The normalised losses of B and Li closely track each other and after an initially rapid loss up to 14 days the normalised losses reduce slightly to NL_B and NL_{Li} = ~1.5 g m^{-2}. The normalised mass loss of Na increases up to 56 days after which it stabilises at NL_{Na} = ~1 g m^{-2}. The normalised loss of Ba steadily decreases from ~0.5 g m^{-2} at 14 days to 0.02 g m^{-2} at 56 days after which the normalised loss stabilises. Ca, Si and Al show similar leaching behaviour to Ba, albeit with normalised loss values that are at least one order of magnitude less. Meanwhile, for the elements sourced from the waste simulant, considerable Cs leaching occurred, with NL_{Cs} being 0.30±0.04 g m^{-2} after 180 days contributing to about 8% of the total NL (~4.0 g m^{-2}), while Sr leached to a much lesser extent (NL_{Sr} = $1.97 \pm 0.22 \times 10^{-3}$ g m^{-2}); Mg and Ce were not detected (<0.01 ppm) in the leached solutions.
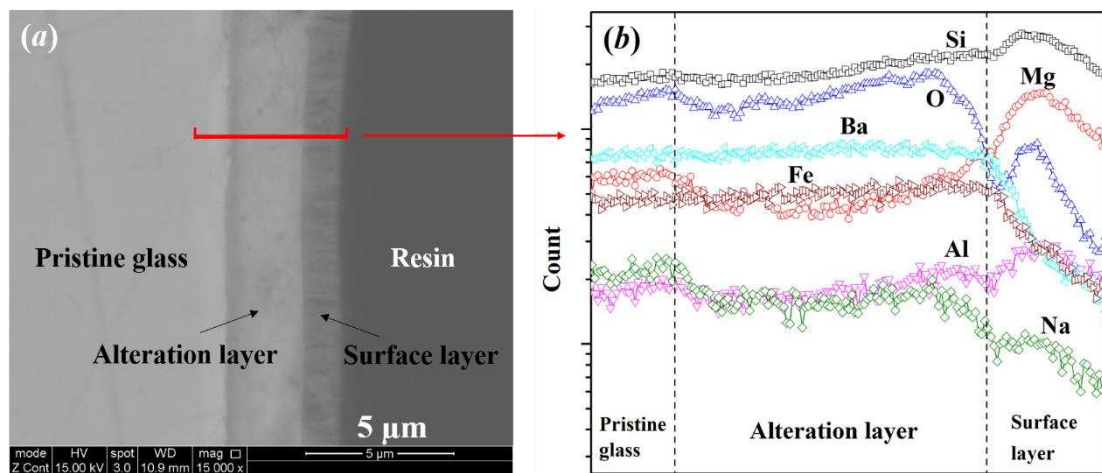
3.4.2. Surface layers

Fig. 9 Cross section of leached glass powder (90 days PCT-B): (a) BSE image and (b) linescan across the surface area.

The glass powders develop two distinct layers on the surface after 7 days of leaching test. Fig. 9a shows a BSE image of a typical cross section of a leached glass powder

(90 days PCT-B), showing an alteration layer on the surface of the unaltered bulk glass and a further surface layer on top of the alteration layer. According to the EDS line scan (Fig. 9b), the alteration layer contains slightly lower amounts of Si, O, Mg, Al and Na than the pristine glass at the transition boundary between these two regions. However the levels of these elements in the alteration layer gradually increase to levels equal to or greater than those in the pristine glass as the surface layer is approached. Meanwhile, the surface layer contains increased amounts of Mg, Si and Al compared to the pristine glass. It is not clear why the surface layer has a reduced O content compared to the pristine glass, although the O signal does follow the same pattern as other elements within this layer. The surface layer is therefore believed to be made up of magnesium (alumino-)silicate phases. While the thickness of the alteration layer increases with dissolution time the thickness of the outer surface layer is between 1.5 and 2 µm and does not change significantly throughout the test.

3.4.3. Crystalline alteration products formed during leaching

XRD (Fig. 10) detected the formation of crystals on the glass after 7 days in the PCT-B test. The intensities of crystalline peaks increased from 7 to 28 days and did not change further, suggesting that the crystallisation process may have reached a limit after 28 days. These crystals are identified as orthorhombic $BaCO_3$ (PDF4#00-005-0378, plotted in the bottom of Fig. 10). SEM images of directly-dried leached glass powders (Fig. 11a and b) confirm the formation of crystals on the surface: needle-like $BaCO_3$ particles (based on the identification of Ba by EDS) are randomly and sparsely distributed on the surface of some of the powder particles. Additionally, a small amount of plate-like particles, which contain Ba, S and O, are observed on a few glass powder surfaces (Fig. 11c); S originates from the waste (see Table 1). This phase is

likely to be $BaSO_4$, and is possibly responsible for the tiny peaks at $2\theta = 24.1°$ and 24.5° of XRD patterns in Fig. 10.
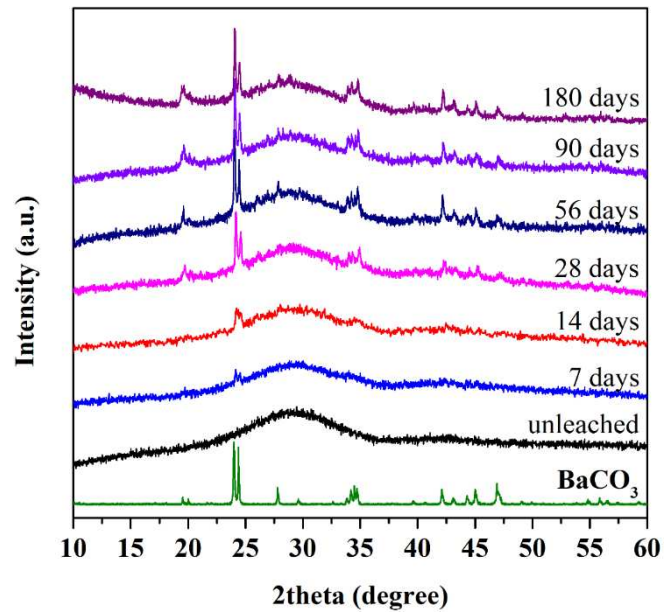

Fig. 10 XRD patterns of HM09-30MS glass powders with increasing PCT-B duration.
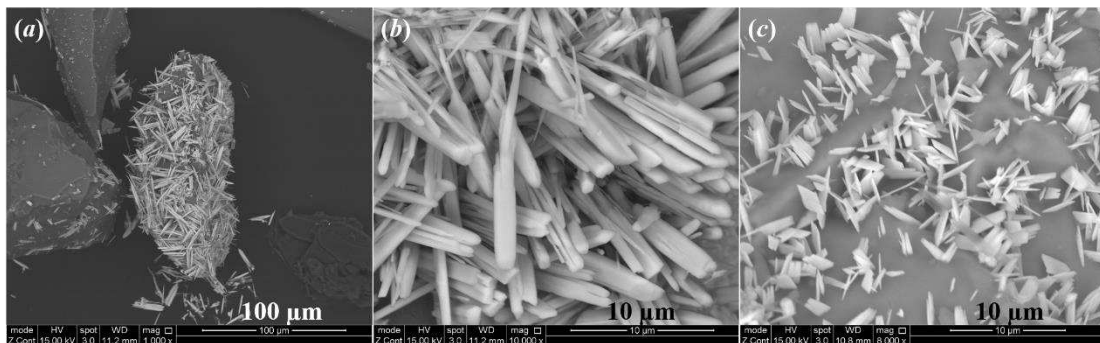
Fig. 11 SEM images of leached glass powders (after 14 days PCT-B). (*a*) One powder covered by crystals, (*b*) needle-like crystals and (*c*) plate-like crystals on powders.

4. *Discussion*

4.1. Loading capacity and phase separation

In order to achieve homogeneous glass products the loading of the simulant Magnox sludge in the HM09 glass composition needs to be 30 wt% or lower. Excess loading results in the formation of separated phases within the glass: forsterite (Mg_2SiO_4)

firstly separates out, while additional CeO_2 and spinels ($MgFe_2O_4$) begin to appear at higher loading levels. Therefore incorporation of the high Mg content in the waste is the controlling factor that limits waste loading in the glass.

4.2. Mg metal dissolution

The presence of residual Mg particles observed in HM09-40MS and -45MS suggests that not all of the Mg particles present in the waste can dissolve into the melt as the waste loading increases. However, Mg particles are only found when the glass has already phase separated due to the formation of forsterite; all of the undissolved Mg particles are entrapped in forsterite clusters. It is likely that the clusters of forsterite plate clusters obstruct the contact between the enclosed Mg granules (if any) and glass melt during melting, thereby leading to incomplete dissolution of the Mg granules. The amount of forsterite in the HM09-35MS sample is still low and therefore no undissolved Mg/MgO particles are entrapped. Thus initially Mg granules can be successfully oxidised into the melt, however eventually saturation of the melt in Mg around the dissolving granules results in the formation of forsterite clusters which prevent further dissolution of the Mg. In an actual melting system this could potentially be addressed by the addition of agitators to prevent local Mg saturation around the dissolving granules.

4.3. Volatiles

~90% retention of Cs_2O in the simulant waste was achieved independently of the waste loading. It is therefore reasonable to assume that the Cs retention when dealing with the target waste stream will not be less than 90 wt% assuming equivalent melting conditions. Considering that the amount of Cs_2O added to the simulant waste in this study (0.5 wt%) was ~500× greater than that in the target waste stream, in principle

the glass must be able to accommodate all of the Cs in the waste at a 30 wt% waste loading. In practice the actual amount retained may also be affected by the melting technology used, for example a cold cap melter would minimise the potential for volatilisation, as would minimising the melt surface area to volume ratio.

In comparison, about 40% of chlorine added to glass has been lost after melting, which is similar to our previous studies of chlorine dissolution in borosilicate glasses [23]. Moreover, the significant chlorine loss in HM09-40MS suggests that the occurrence of phase separation in the melt may accelerate Cl evaporation during melting. Although Cl volatilisation poses challenges to the off-gas system of a thermal processing unit as wet Cl_2 gas is highly corrosive, it is not in itself part of the radiological inventory of the waste. Thus, depending on what other species get carried over into the off-gas with the Cl, retention may not be essential.

The measured SrO content was constant and was higher than the expected values in all waste-loaded glasses. Given the fact that a small amount of SrO was also found in the base glass, it is likely that the glass raw materials, probably the significant amount of $BaCO_3$, contain some impurities of Sr salts, which contributed to the SrO content in the final glasses. This results in difficulty in analysing volatilisation of Sr in glass, although assuming a constant ratio of Sr to Ba from the base glass components suggests that all the Sr is retained, except in the HM09-40MS glass where the retention rate appears to be ~80-85%.

4.4. Effect of waste loading on glass properties

The addition of waste simulant to HM09 glass does not cause any notable changes in the XRD patterns and Raman spectra at lower waste loadings. This suggests that the dissolved waste constituents have been incorporated into the glass network rather than

being present separately within the glass matrix. Also, even at higher waste loadings where the glass becomes heterogeneous the glassy part of products retain the same features. The steady increase of T_g with increasing waste loading indicates that the energy required for glass structural relaxation is increased due to incorporation of significant amounts of Mg into the glass.

4.5. Glass durability

In common with most waste glasses the leaching of Li, B and Na is initially rapid but this rate then drops (up to a period of 180 days), which indicates a transition to a "final" rate regime. The decay in the NL_{Ba} values can be explained by the formation of $BaCO_3$ crystals on the glass particle surfaces during the PCT-B test: the reaction between Ba^{2+} (leached to solution) and CO_3^{2-} (from dissolved CO_2 in water) to form insoluble $BaCO_3$, results in significant consumption of Ba^{2+} from solution. This could potentially be due to the removal of all the dissolved CO_2 in the static solution, although it should be noted that the tests were not conducted in a CO_2 free glovebox. The possible $BaSO_4$ phase will also consume Ba^{2+} from solution, albeit to a much lesser extent. However according to the XRD and SEM results, the formation of insoluble Ba salts does not increase after NL_{Ba} has become constant suggesting that further leaching of Ba^{2+} is prevented.

Meanwhile, the observed magnesium (alumino-)silicate surface layer is X-ray amorphous. The formation of such precipitates has been previously reported by Curti *et al.* [24] when assessing the Mg-bearing MW high level nuclear glass and by Debure *et al.* [25] and Fleury *et al.* [26] when assessing the French reference nuclear glasses with deliberate addition of Mg^{2+} source to the leaching solutions. Similar to the findings in references [24], [25] and [26], magnesium silicate precipitates begin to form as soon as the experiment starts, giving rise to the low NL_{Si} and negligible NL_{Mg}

values. It appears that the formation of these precipitates does not detrimentally affect the overall leaching behaviour of the glass.

The leaching of Cs follows similar patterns to that of Na and Li, with a stable NL_{Cs} value of 0.30 g m^{-2} for 56-180 days; unfortunately Cs in solution was not measured for the 7, 14 and 28 day samples so it is not possible to state how quickly NL_{Cs} reaches a value of 0.30 g m^{-2}. The leaching of Cs is potentially of concern due to the significant contribution of Cs to the activity of the waste. More significantly the two major Cs isotopes contributing to the activity of the waste namely [134]Cs and ^{137}Cs have half-lives of 2.0652 y and 30.08 y respectively [27] which means that >10 half-lives should have passed and thus the levels of these isotopes should be negligible (although long-lived [135]Cs would remain), before water ever reaches the glass in any disposal scenario being proposed for UK ILW. Thus, except in an extreme fault scenario, the relative ease by which Cs may be removed from the glass through leaching should not be a problem. The high initial retention level for Cs in the glass is more significant as minimising the amount of Cs that goes into the off-gas is always a challenge for thermal treatment routes.

Given that Ce was used to simulate the actinides present in the waste it is reassuring that no Ce was detected in the leachates after testing for time periods up to 180 days. While strictly this only shows that Ce is not leached from the glass it may give some indication that the long-lived actinide species would also be retained in the glass under long term disposal conditions. It should be noted however that Ce will most likely not be in the same oxidation as U in the glass; for air-melted glasses it has been found that U is likely to be present as U^{6+} in uranyl ions sitting in modifier channels in the glass structure [28], [29] and [30]. Thus differences in leaching behaviour could be expected although Greaves *et al.* [30] found that U leached out of the glass

reprecipitated as hydrated uranyl silicate complexes on glass surface inhibiting further dissolution of uranium. In addition, of course, the multi-barrier concept is designed to prevent any species that do leach out of the wasteform from making it back to the biosphere.

5. Conclusions

A novel iron containing borosilicate glass composition that shows potential for the immobilisation of Magnox sludge waste, which includes both metallic and oxides/hydroxide phases has been developed. The glass can incorporate up to 30wt% (dry weight) of a simulant Magnox sludge into a homogeneous product. Up to 90% of the Cs spike used (>500× the actual Cs content in the waste) was retained in the glass thus under the right processing conditions the glass has the potential to retain all of the Cs in the waste. ~40% Cl was lost during glass melting, which would have to be dealt with in the off-gas of any industrial process replicating this experiment, however Cl is not part of the radiological inventory of the waste. If >30 wt% waste was added then saturation of the melt locally in Mg led to the formation of forsterite around the residual Mg metal in the final wasteform.

Leaching for time periods of up to 180 days followed a conventional pattern with an initial higher rate of leaching followed by a rate reduction which reflected the formation of an amorphous magnesium (alumino-)silicate hydrated layer on the glass surface. No Ce (representing the long-lived actinide content) was leached from the glass. and although Cs was leached from the glass this is not seen as a serious problem due to the relatively short half-lives of the isotopes concerned.

Data availability

The data that support the findings of this study are available from the corresponding author upon reasonable request.

References

1.   Donald, I.W., *Waste immobilisation in glass and ceramic based hosts: radioactive, toxic and hazardous wastes*. 2010: Wiley-Blackwell.

2.   NDA, *2016 UK Radioactive Waste & Materials Inventory: UK Radioactive Waste Inventory Report*. 2017: NDA. p. 205.

3.   Bingham, P.A., N.C. Hyatt, and R.J. Hand, *Vitrification of UK intermediate level radioactive wastes arising from site decommissioning: property modelling and selection of candidate host glass compositions*. Glass Technology - European Journal of Glass Science and Technology Part A, 2012. **53**(3): p. 83-100.

4.   Ojovan, M.I., *Handbook of Advanced Radioactive Waste Conditioning Technologies*. 2011: Woodhead Pub.

5.   Sharp, J.H., et al. *Cementitious systems for encapsulation of intermediate level waste*. in *The 9th International Conference on Radioactive Waste Management and Environmental Remediation*. 2003. Oxford.

6.   Bart, F., et al., *Cement-based materials for nuclear waste storage*. 2013, London: Springer.

7.   Ojovan, M.I. and W.E. Lee, *An Introduction to Nuclear Waste Immobilisation*. 2005, Amsterdam: Elsevier.

8.   Lutze, W. and R.C. Ewing, *Radioactive Wasteforms for the Future*. 1988, Amsterdam: North Holland.

9.   Sobolev, I.A., et al., *Vitrification processes for low, intermediate radioactive and mixed wastes*. Glass Technology, 2005. **46**(1): p. 28-35.

10.   Ojovan, M.I. and W.E. Lee, *Glassy Wasteforms for Nuclear Waste Immobilization*. Metallurgical and Materials Transactions A, 2010. **42**(4): p. 837-851.

11.   Lee, W.E., et al., *Immobilisation of radioactive waste in glasses, glass composite materials and ceramics*. Advances in Applied Ceramics, 2006. **105**(1): p. 3-12.

12.   Gin, S., et al., *An international initiative on long-term behavior of high-level nuclear waste glass*. Materials Today, 2013. **16**(6): p. 243-248.

13.   Heath, P.G., et al., *Hot-isostatically pressed wasteforms for Magnox sludge immobilisation*. Journal of Nuclear Materials, 2018. **499**: p. 233-241.

14.   Lenoir, M., et al., *Quantitation of sulfate solubility in borosilicate glasses using Raman spectroscopy*. Journal of Non-Crystalline Solids, 2009. **355**(28-30): p. 1468-1473.

15.   Koroleva, O.N., L.A. Shabunina, and V.N. Bykov, *Structure of borosilicate glass according to raman spectroscopy data*. Glass and Ceramics, 2011. **67**(11-12): p. 340-342.

16.   Yadav, A.K. and P. Singh, *A review of the structures of oxide glasses by Raman spectroscopy*. RSC Advances, 2015. **5**(83): p. 67583-67609.

17. Chopelas, A., *Single crystal Raman spectra of forsterite, fayalite and monticellite.* American Mineralogist, 1991. **76**: p. 1101-1109.

18. McKeown, D.A., M.I. Bell, and R. Caracas, *Theoretical determination of the Raman spectra of single-crystal forsterite (Mg2SiO4).* American Mineralogist, 2010. **95**(7): p. 980-986.

19. Venugopal, A.K., et al., *Oxidative dehydrogenation of ethyl benzene to styrene over hydrotalcite derived cerium containing mixed metal oxides.* Green Chemistry, 2013. **15**(11): p. 3259.

20. Cui, J. and G.A. Hope, *Raman and Fluorescence Spectroscopy of CeO2, Er2O3, Nd2O3, Tm2O3, Yb2O3, La2O3, and Tb4O7.* Journal of Spectroscopy, 2015. **2015**: p. 1-8.

21. D'Ippolito, V., et al., *Raman fingerprint of chromate, aluminate and ferrite spinels.* Journal of Raman Spectroscopy, 2015. **46**(12): p. 1255-1264.

22. da Silva, S.W., et al., *Raman study of cations' distribution in Zn x Mg1−x Fe2O4 nanoparticles.* Journal of Nanoparticle Research, 2012. **14**(4).

23. Tan, S., *The incorporation and solubility of sulphate, chloride and molybdate anions in borosilicate and aluminosilicate glasses*, in *Department of Materials Science and Engineering*. 2015, The University of Sheffield: Sheffield. p. 252. http://etheses.whiterose.ac.uk/id/eprint/9990

24. Curti, E., et al., *Long-term corrosion of two nuclear waste reference glasses (MW and SON68): A kinetic and mineral alteration study.* Applied Geochemistry, 2006. **21**(7): p. 1152-1168.

25. Debure, M., et al., *Borosilicate glass alteration driven by magnesium carbonates.* Journal of Nuclear Materials, 2012. **420**(1-3): p. 347-361.

26. Fleury, B., et al., *SON68 glass dissolution driven by magnesium silicate precipitation.* Journal of Nuclear Materials, 2013. **442**(1-3): p. 17-28.

27. *Chart of Nuclides*. 2018 [accessed 2018 2018-07-20]; Available from: http://www.nndc.bnl.gov/chart/.

28. Farges, F., C.W. Ponader, and G.E. Brown, *Structural environments of incompatible elements in silicate glass/melt systems: II U^{IV}, U^{V} and U^{VI}.* Geochimica et Cosmochimica Acta, 1992, **56**, p. 4205-4220

29. Greaves, G.N., et al., *Glancing-angle X-ray absorption spectroscopy of corroded borosilicate glass surfaces containing uranium.* Journal of the American Chemical Society, 1989, **111**, p. 4313-4324.

30. Connolly, A.J., et al., *The effect of uranium oxide additions on the structure of alkali borosilicate glasses*. Journal of Non-Crystalline Solids, 2013, **378**: p. 282-289.